Experimental analysis and numerical modelling of an AQSOA zeolite desiccant wheel

Manuel Intini [a,*], Mark Goldsworthy [b], Stephen White [b], Cesare Maria Joppolo [a]

[a] Dipartimento di Energia, Politecnico di Milano, Via Lambruschini, 4, 20156 Milan, Italy
[b] CSIRO Energy Technology, 10 Murray Dwyer Circuit, Mayfield West, 2300 NSW, Australia

Received 5 June 2014
Accepted 13 January 2015
Available online 22 January 2015

1. Introduction

Desiccant wheels are key components for desiccant cooling systems with low grade thermal activation energy. This makes them appealing devices for solar thermal applications and cogeneration systems in which low temperature heat can be recovered. The overall design of desiccant cooling systems requires simultaneous optimization of a number of parameters [1] (area ratio, regeneration temperature, surface velocity, revolution speed). Use of simulation tools calibrated with limited experimental measurements is a practical and cost effective approach for energy simulation analysis [2].

Silica gel is one of the best performing and commonly investigated materials in desiccant wheels owing to its good long term stability and minimal hysteresis. Kodama et al. [3,4] investigated performance of rotary adsorbents focussing on fractional residual of water vapour and optimal revolution speed. Silica gel-based adsorbents, both as pure [5] and compound forms [6] have been widely characterized in terms of adsorption equilibrium and diffusivity. Recently interest has risen in alternative desiccant materials with higher moisture uptakes even at low regeneration temperature. Aristov et al. found out that moisture uptake on hygroscopic salts can be significantly higher than pure silica gel [7,8]. Zhang [9] and Ge [10] investigated the increase in performance of desiccant wheels in which silica gel based adsorbent is mixed with calcium and lithium chloride respectively. Zeolites are common alternative to silica gel since they are quite widespread for many chemical uses and can be synthesized according to application requirements. Conventional zeolites, such as Type A and Type Y, show a typical S-shape adsorption isotherm which is ideally suited for dehumidification and drying processes. However, their adsorption isotherm generally has a zone of steepest

* Corresponding author. Tel.: +39 0223993874.
E-mail address: manuel.intini@polimi.it (M. Intini).

gradient in the low humidity range, i.e., the minimal amount of adsorbed water vapour is achieved only at extremely low relative humidity. It follows that maximum differential uptake is obtained only with very high regeneration temperatures (typically 120–250 °C [11,12]). A new generation of AQSOA™ (Aqua Sorb Adsorbent) zeolites, recently developed by *Mitsubishi Plastics Inc.*, is an interesting solution to exploit low grade heat. AQSOA consists of crystalline silico-alumino-phosphate materials with a CHA structure [13]. With this new generation of zeolites, the steepest gradient zone of the adsorption isotherm can be shifted towards higher relative humidity values [14] compared with conventional zeolites such as Type A or Type Y [15]. Dehumidification performance can be even comparable with common desiccant materials such as silica gel regenerated with low and medium regeneration temperatures.

A preliminary assessment of moisture removal capacity can be based on moisture differential uptake $\Delta W_{ads,\ i.e.}$, the difference between water vapour uptake evaluated at process inlet and regeneration inlet relative humidity conditions respectively. This would be ideally the maximum amount of water removed per unit mass of desiccant if the adsorbent achieved equilibrium with inlet air flows. As it is shown in Fig. 1 given a pair of reference process and regeneration temperatures with the same humidity ratio (T_{pro} 30 °C, RH_{pro} 50% and T_{reg} 80 °C RH_{reg} 4.5% respectively) the moisture differential uptake may be even larger in AQSOA-based desiccant than a silica gel-based one. Silica gel isotherms [16] have limited dependency on temperature, so that adsorption equilibrium curves can be considered almost overlapping in the RH-W chart (Fig. 1).

This new generation of zeolites has been raising interest both in adsorbent characterization and cooling applications. Goldsworthy [17] has recently compared different kind of AQSOA zeolites for modelling of adsorption chillers and desiccant wheels. Frazzica [18] adopted a new experimental protocol to evaluate thermodynamic performance of AQSOA-Z02 as a desiccant for advanced working pair in adsorptive heat transformers. Dawoud [19] provided an insight into water vapour adsorption kinetics on small AQSOA-Z02-coated aluminium substrates for adsorption heat exchangers. Plenty of experimental results are available on alternative desiccant materials [20], however only few authors dealt with new generation of zeolites [21,22] and neither a comprehensive nor a model driven numerical analysis has been carried out on AQSOA zeolite-based desiccant wheels.

In the present work, an AQSOA-Z02 desiccant wheel is investigated both numerically and experimentally. First, a brief introduction to the desiccant wheel test facility is provided, including details on the measuring process and uncertainty analysis. Then, a time dependent numerical model is described and calibrated on experimental data. The model is adopted to investigate wheel performance on out of testing range conditions.

2. Experimental setup

Tests on an AQSOA desiccant wheel have been performed using the Controlled Climate Test Facility at the CSIRO Energy Centre in Newcastle. A schematic is provided in Fig. 2. The facility is designed to provide two air streams at accurate controlled conditions of temperature and humidity. The former stream simulates the fresh supply air, mainly referred as the *process flow*, which is to be dehumidified by the test desiccant wheel. The latter stream is a relatively high temperature air flow that regenerates the desiccant and is referred to as the *regeneration flow*.

Process and regeneration air streams are then ducted to the desiccant wheel test bench in counter flow arrangement. The supply and regeneration air streams leaving the desiccant wheel are ducted from the wheel and exhausted outside. Data acquisition and system control is programmed via LabVIEW 7.1. Measurement sensors in the test facility are described below;

- Temperature is measured with class B RTD sensors, with accuracy a function of temperature as follows $\delta T = 0.005T + 0.3$ (T and δT in °C).
- Relative humidity is measured with capacitive sensors with accuracy ±1.3%RH and with two high accuracy Optica chilled mirror hygrometers. The four air flows are each sampled by sampling tree located in each of the wheel inlet and outlet ducts. The resulting dew point temperature can be measured with an accuracy of 0.2 °C.
- Volume flow rate is measured downstream with Pitot tube anemometer. Pressure drop across the nozzles is measured by

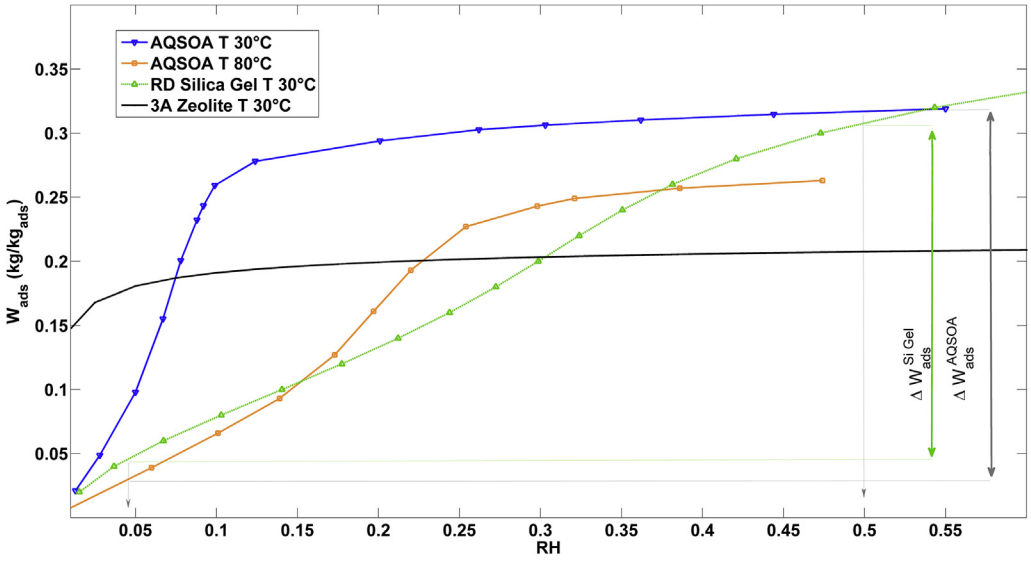

Fig. 1. Comparison of Novel AQSOA Zeolite Isotherms (data extrapolated from Kakiuchi [14]) with regular density silica gel [16] and 3A Zeolite isotherms [15].

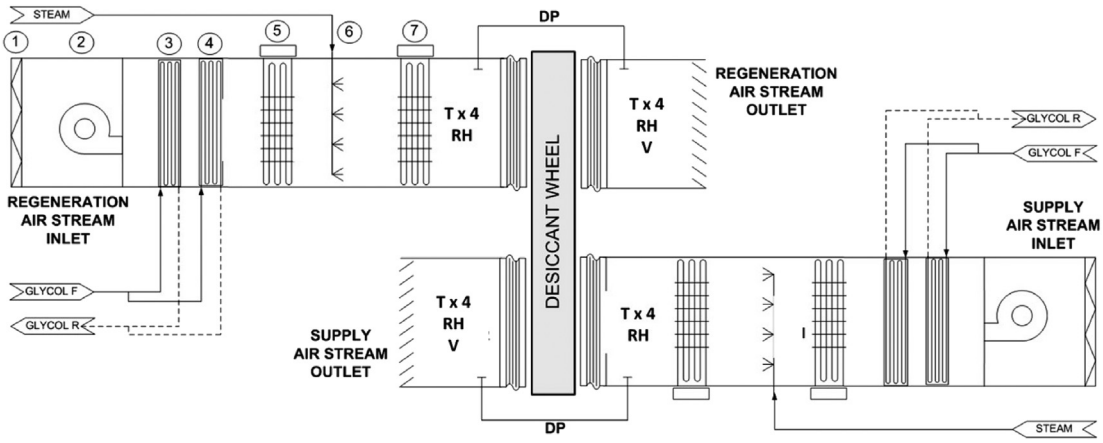

Fig. 2. A schematic of CSIRO experimental facility. (1) Intake filter, (2) Fan, (3) Medium temperature coil, (4) Low temperature coil, (5) Primary heater bank, (6) Steam injection humidifier, (7) Secondary heater bank, (T) Temperature sensor, (RH) Relative humidity sensor, (V) Velocity sensor, (DP) Differential pressure sensor.

differential pressure transmitters with accuracy of ±0.62 Pa. Mass flow rate is then calculated by gathering density from temperature and relative humidity at the nozzle inlet section.

Further details about the facility can be found in White et al.[21]. Experimental results are provided in Section 4.

3. Desiccant wheel numerical model: governing equations

A time dependent finite-difference model has been developed to predict wheel outlet temperature and humidity ratio as a function of inlet conditions. In the model the desiccant wheel is reduced to an equivalent sinusoidal channel in which heat and moisture transfer occur between the air flow and desiccant. Continuity and energy equations are solved both for air flow and solid desiccant. According to Ge's classification [23], the current model can be referred to as a quasi-Gas and Solid Side Resistance Model since thermal conduction is taken into account but neither adsorbed water nor water vapour diffusion in the wall is considered. Here follow the main assumptions:

- *Equivalent channel reduction*: desiccant wheel is reduced to an equivalent sinusoidal channel and each channel is not affected by adjacent ones
- *Inlet airflow conditions*: uniform distribution of u, T_a and x_a is assumed for both process and regeneration cycle
- *Diffusion mechanisms in the media*: surface diffusion for adsorbed water and combination of ordinary and Knudsen for water vapour diffusion is considered
- *Adsorbed water equilibrium*: water vapour mass fraction in the solid media is calculated as a function of desiccant isotherm adsorption equilibrium
- *Space discretization*: only axial direction is considered, temperature, humidity ratio and adsorbed water gradients in radial and circumferential directions are neglected

The set of governing equations includes water vapour continuity in the air flow (Eq. (1)), wet air energy balance (Eq. (2)), water vapour and adsorbed water continuity in the solid side (Eq. (3)) and energy balance in the solid medium (Eq. (4)).

$$\rho_a \frac{\partial x_a}{\partial t} + \rho_a u \frac{\partial x_a}{\partial z} = \frac{h_M (x_d - x_a)}{A_c/P} \tag{1}$$

$$\rho_a (c_{Pa} + x_a c_{Pw}) \left[\frac{\partial \check{T}_a}{\partial t} + u \frac{\partial \check{T}_a}{\partial z} \right] = \frac{h_T (\check{T}_d - \check{T}_a)}{A_c/P} \tag{2}$$

$$\rho_a \varepsilon \frac{\partial x_d}{\partial t} + \rho_s (1-\varepsilon) f_D \frac{\partial W}{\partial t} = \rho_a \varepsilon D_G \frac{\partial^2 x_d}{\partial z^2} + \rho_s (1-\varepsilon) D_S \frac{\partial^2 W}{\partial z^2} + \frac{h_M (x_a - x_d)}{A_s/P} \tag{3}$$

$$\rho_s (c_{Ps} + f_D W c_{Pw}) \frac{\partial \check{T}_d}{\partial t} = k_s \frac{\partial^2 \check{T}_d}{\partial z^2} + \frac{[h_T (\check{T}_a - \check{T}_d) + h_M (x_a - x_d) Q_{st}]}{A_s/P} \tag{4}$$

Initial conditions are set as follows (Eqs. (5)–(7)):

$$\check{T}_a(z,0) = \check{T}_d(z,0) = \check{T}_{reg}^{in} \tag{5}$$

$$x_a(z,0) = x_d(z,0) = x_{reg}^{in} \tag{6}$$

$$W(z,0) = W_{reg} \tag{7}$$

being W_{reg} the amount of water adsorbed when the desiccant is in equilibrium with a moist air flow at regeneration inlet temperature and humidity ratio. W_{reg} is calculated according to Eqs. (14)–(15).

The set of equations is solved given the following initial and boundary conditions (Eqs. (8)–(13))

$$\left.\frac{\partial W}{\partial z}\right|_{z=0} = \left.\frac{\partial W}{\partial z}\right|_{z=L} = 0 \tag{8}$$

$$\left.\frac{\partial \check{T}_d}{\partial z}\right|_{z=0} = \left.\frac{\partial \check{T}_d}{\partial z}\right|_{z=L} = 0 \tag{9}$$

$$\left.\frac{\partial \check{T}_a}{\partial z}\right|_{z=0} = \left.\frac{\partial x_a}{\partial z}\right|_{z=0} = 0 \quad 0 < t \le \tau_{pro} \tag{10}$$

$$\left.\frac{\partial \check{T}_a}{\partial z}\right|_{z=L} = \left.\frac{\partial x_a}{\partial z}\right|_{z=L} = 0 \quad \tau_{pro} < t \le \tau_{cyc} \tag{11}$$

$$\check{T}_a\big|_{z=0} = \check{T}_{pro}^{\,in}, \quad x_a|_{z=0} = x_{pro}^{in} \quad 0 < t \le \tau_{pro} \tag{12}$$

$$\check{T}_f\Big|_{z=L} = \check{T}_{reg}^{\,in} \quad x_a|_{z=L} = x_{reg}^{in} \quad \tau_{pro} < t \le \tau_{cyc} \tag{13}$$

The amount of water vapour content at the interface is calculated by the FAM AQSOA isotherm equilibrium curve. Experimental data are known at three different reference temperatures [14]. Toth's formulation (Eq. (14)) is adopted to fit experimental data provided by Kakiuchi et al. [14], being p_v the partial pressure of water vapour in the flow and T_D the desiccant layer temperature. Since adsorption and desorption curves are almost overlapping no hysteresis has been assumed.

$$W = \frac{k_0 p_v \exp[Q_{st}/R\check{T}_d]}{\left[1 + \left(\frac{k_0 p_v \exp[Q_{st}/R\check{T}_d]}{W_{max}}\right)^n\right]^{1/n}} \tag{14}$$

Values of k_0, W_{max} and n are fitted to experimental data and provided in Table 1 with a normalized root mean square deviation of 8.65%. Heat of adsorption Q_{st} is assumed constant and provided in Table 2. Little discrepancy is observed at 10 °C isotherm, however no simulations have been performed in such a low range of temperatures. Linear interpolation and extrapolation for coefficients n and W_{max} has been assumed for 10 °C < T ≤ 90 °C and for T > 90 °C respectively.

Water vapour partial pressure is then linked to humidity ratio with Eq. (15) and assuming p_{atm} equal to 101,325 Pa. The effect of pressure loss across the wheel is neglected.

$$x_d = \frac{0.622 p_v}{p_{atm} - p_v} \tag{15}$$

In Equations (3)–(4) cp_s, ρ_s, k_s and ε are the equivalent specific heat, true density, thermal conductivity and void fraction of the solid media (matrix + desiccant) and they are assumed equal to the pure desiccant values due to the high level of desiccant mass fraction in the channel. In particular the solid media bulk density defined as in Eq. (16) is assumed to be equal to the AQSOA powder density provided by Kakiuchi et al. [14].

$$\rho_s^b = (1 - \varepsilon)\rho_s \tag{16}$$

Diffusivity of water vapour is the combination of ordinary and Knudsen diffusion, since both mechanisms exist. Equations (17)–(19) are widely adopted to calculate diffusion quantities in water vapour diffusion phenomena [10,24]:

$$D_G = \left(\frac{1}{D_o} + \frac{1}{D_{kn}}\right)^{-1} \tag{17}$$

$$D_o = 1.735 \cdot 10^{-9} \frac{T_d^{1.685}}{p_v} \tag{18}$$

Table 1
Equilibrium isotherm coefficients fitting.

	T 10 °C	T 50 °C	T 90 °C
k_0 [kPa^{-1}]	2.8E-11	2.8E-11	2.8E-11
n	1.6	3.5	5
W_{max} [kg/kg]	0.34	0.31	0.27

Table 2
Thermodynamic properties adopted in the model.

Property	Value	Reference
ρ_s^b [kg m^{-3}]	650	[14]
C_{ps} [J kg^{-1} K^{-1}]	900	[14]
D_s [m^2 s^{-1}]	4.9E-12	[25]
r_p [nm]	0.19	[14]
ε	0.45	Assumed
f_D [kg kg^{-1}]	0.88	Fitted to experimental data
Nu_{fd}	2.4	[26]
Q_{st} [kJ kg^{-1}]	3378	[14]

$$D_{kn} = 97 r \left(\frac{T_d}{MM}\right)^{0.5} \tag{19}$$

being r the pore radius and MM the water vapour molar mass, equal to $1.9 \cdot 10^{-10}$ m and 18 kg kmol^{-1} respectively. Effective surface diffusivity has not been measured for AQSOA zeolite, therefore diffusivity of a standard 3A zeolite [25] is assumed. Heat and mass transfer coefficients h_T and h_M are calculated by Nusselt and Sherwood number, defined in Eqs. (20)–(21)

$$Nu = \frac{h_T D_H}{k_a} \tag{20}$$

$$Sh = \frac{h_M D_H}{\rho_a D_o} \tag{21}$$

Fully developed Nusselt number Nu_{fd} is assumed to 2.4 according to Kacaç et al. [26,27] as the current heat transfer phenomenon can be considered neither as constant temperature nor as constant heat flux case. In order to consider the temperature profile developing length Graetz number is used [28] to calculate the local Nusselt number (Eq. (22))

$$Nu_x = Nu_{fd} + \frac{0.0841}{0.002907 + Gz^{-0.6504}} \tag{22}$$

being local Gz number defined in Eq. 23

$$Gz = RePr \frac{D_H}{z} \tag{23}$$

Assuming Le = 0.87 [26] and applying Chilton–Colburn Analogy Le is approximately 1 (Eq. (24))

$$Le^{1/3} = \frac{Nu}{Sh} \approx 1 \tag{24}$$

therefore Sherwood is equal to Nusselt number.

Hydraulic diameter depends on channel geometry and it is calculated according to Kakaç formulation [27] for sinusoidal channels (Eq. (25))

$$D_H = a\left[1.0542 - 4.670\left(\frac{a}{b}\right) - 0.1180\left(\frac{a}{b}\right)^2 + 0.1794\left(\frac{a}{b}\right)^3 - 0.0436\left(\frac{a}{b}\right)^4\right] \tag{25}$$

In order to predict the outlet flow conditions the time-averaged conditions are computed at the end of each half cycle (process or regeneration cycle) defined as in Eq. (26).

Table 3
Novel zeolite desiccant wheel geometry details.

Geometrical feature	Value
Wheel outer diameter [mm]	320
Wheel hub diameter [mm]	38
Channel height a [mm]	1.5
Channel width b [mm]	3.4
Wall half thickness c [mm]	0.13

$$\Psi_{ave} = \frac{1}{\tau}\int_0^{\tau} \Psi_{(\hat{z},t)}\,dt \tag{26}$$

Being $\hat{z}$ the outlet axial coordinate, τ either process or regeneration stage time and Ψ the general outlet flow quantity (temperature or humidity ratio). Stationary conditions are assumed as time averaged outlet quantities do not vary more than a fixed tolerance of 1%.

Geometrical data (Table 3) have been directly gathered on the actually tested wheel manufactured by *Mitsubishi Plastics*. Channel quantities have been averaged on 20 samples picked at different radial location.

Equations are solved with Implicit Euler Scheme. A minimum time step equal to 0.02 s has been found to guarantee solution stability, while a space step of 0.005 m turns out to be a reasonable value to achieve solution grid-independency.

The equations were discretised using the implicit backward Euler Scheme. Equations are solved assuming constant thermodynamic properties, i.e., diffusivity of water vapour D_G, moist air specific heat capacity and desiccant specific heat capacity. These parameters have been evaluated at temperature $\breve{T}_{ave}$ (the average of process and regeneration air inlet temperature) and adsorbed water content W_{ave} (the average of adsorbed water content at the equilibrium with process inlet flow and regeneration inlet flow respectively). In this way the coefficient matrices were precomputed to save computational time. However, at each time-step the solution was used to iteratively update the value of the desiccant moisture content W according to Eq. (14). As there were typically fewer than 5 iterations required at each time-step, this scheme was thus found to be faster than using an explicit formulation. Although the implicit Euler scheme is unconditionally stable, a minimum time-step of 0.02 s was found to be required to yield stable solutions. A grid sensitivity analysis was conducted and a grid spacing of 0.005 m was found to result in a grid-independent solution. The mathematical model is solved with Matlab© programming language.

4. Experimental results and desiccant wheel model calibration

Experimental results have been collected as a function of air inlet humidity ratio keeping fixed inlet temperatures and mass flow rate. In particular, humidity ratio and face velocity are set equal for both process and regeneration flows. The effect of regeneration temperature is investigated in the low-medium temperature range (60 °C–80 °C) and in the high temperature range (100 °C–120 °C).

Figs. 3 and 4 show the agreement between the numerical model described in Section 3 and experimental results collected. Numerical fitting has been performed on the value of mass fraction of desiccant in the solid media f_D which is provided in Table 2. The root mean square deviation of process outlet humidity ratio and tem-perature is 0.66 g/kg and 0.99 °C respectively. Small discrepancies are observed in Fig. 3 only in the very high inlet relative humidity range (x_{in} >20 g/kg) where the model slightly underestimates the amount of moisture removed. Accordingly, process outlet temperature predicted by the model is lower than experimental data except for the last test (x_{in} = 24.3 g/kg) at T_{reg} 60 °C. This discrepancy may be related to the assumption of constant heat of adsorption which tends to be lower for high adsorbed water content in the desiccant. In fact, at constant process inlet temperature the higher the inlet humidity ratio, the higher the average moisture content in the desiccant, hence the model adopted in this work is likely to overestimate heat of adsorption for very humid inlet conditions and low regeneration temperature.

5. Desiccant wheel performance analysis

In this section desiccant wheel design parameters and effect of flow inlet condition on dehumidification performance are discussed adopting the numerical model discussed in Section 4. Desiccant wheels may be set up with AR >0.5 in order to increase wheel dehumidification capacity, especially when a very high temperature heat source is available for regenerating the desiccant

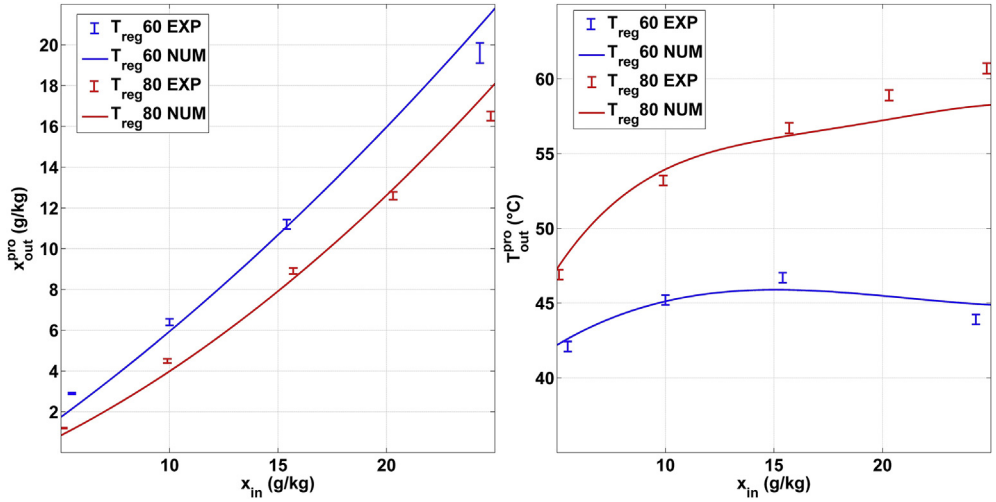

Fig. 3. Comparison of numerical model and experimental data as a function of inlet humidity ratio (low regeneration temperature). Process inlet temperature 30 °C, surface velocity 2 m/s, revolution speed ω 20RPH, AR 0.5.

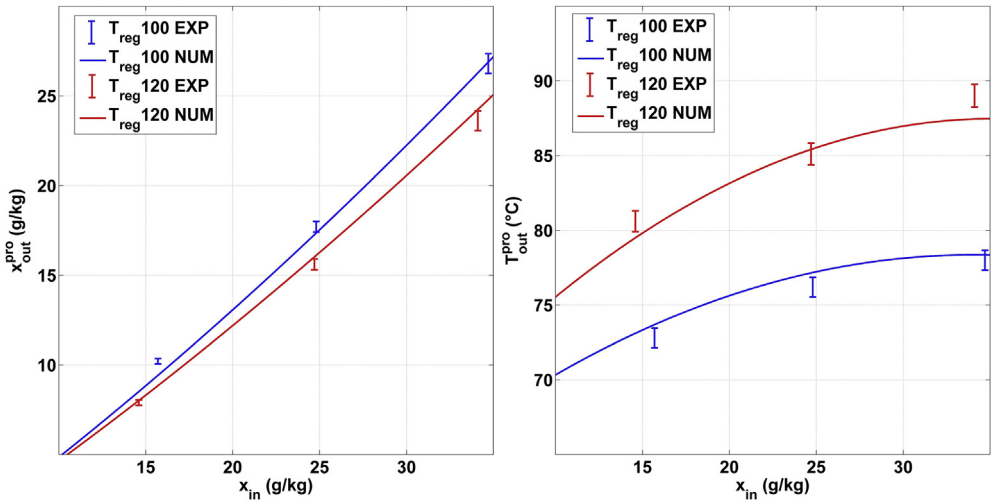

Fig. 4. Comparison of numerical model and experimental results as a function of inlet humidity ratio (high regeneration temperature range). Process inlet temperature T_{pro} 30 °C, surface velocity v 2 m/s, revolution speed ω 20 RPH, AR 0.5.

wheel. If face velocities are kept constant, increasing AR leads to an increase in process air flow rate but, on the other hand, a reduction in humidity ratio drop. Overall desiccant wheel performance is commonly described by the Moisture Removal Capacity (MRC), which is an indicator to assess the latent cooling provided [1,21,29]. The effect on maximum MRC achievable (Eq. (27)) or, equivalently latent cooling in Eq. (28), needs investigating in order to assess the global effect.

$$MRC = m_{pro}\left(x_{pro}^{in} - x_{pro}^{out}\right)\Big/A_{DW} \tag{27}$$

$$Q_{lat} = m_{pro}\left(x_{pro}^{in} - x_{pro}^{out}\right)\Delta H_{ev} \tag{28}$$

Given a set of AR, T_{reg} and process flow inlet conditions, the revolution speed is to be kept close to the value which leads to the maximum MRC. Moreover, desiccant wheels as an integrated component of desiccant cooling system operate far from design conditions for most of the time. Understanding performance variations as a function of outdoor temperature and humidity is fundamental to assess the effective dehumidification for off-peak cooling loads. Lastly, optimal revolution speed may also vary as a function of volume air flow and, therefore, air face velocity, whether part load control implies a variation in volume flow rate.

In this section moist removal performance is investigated as a function of area ratio and humidity ratio drop for different regeneration temperatures. After that, the effect of air inlet conditions is discussed. Finally, an analysis on ω^{opt} as a function of face velocity is provided, highlighting the relation between non-dimensional quantities and optimal revolution speed.

5.1. Effect of area ratio on moisture removal capacity

In order to understand how design conditions affect moisture removal two reference process conditions are hereby considered: a mild outdoor air condition (T_{pro} 30 °C, x_{in} 15 g/kg) and a hot and humid condition (T_{pro} 35 °C, x_{in} 20 g/kg). The analysis is carried out with flow surface velocity equal to 2 m/s in order to find maximum values of MRC that, in turn, is calculated for unitary desiccant wheel cross section area, as shown in Eq. (27).

The mild humidity conditions scenario is provided in Fig. 5. It is found that MRC varies significantly with the amount of process humidity ratio drop required. Each point of the curve represents the highest MRC that is obtained with optimal values of ω and given values of AR and regeneration temperature. Maximum MRC is always increasing with regeneration temperature keeping a fixed humidity ratio drop. However the trend is proved to be less than linear. It is found that maximum MRC is attained with AR 0.5 for low and medium regeneration temperature. Only for very high temperatures (T_{reg} >100 °C) a relatively wide plateau zone is found ranging from 0.5 to 0.6. This behaviour can be explained in the light of two conflicting effects: increasing regeneration temperature a better dehydration of the desiccant occurs in the regeneration stage while a longer precooling time in the process phase is needed prior to adsorption. For T_{reg} at 60 °C, the system is barely useful for air conditioning application since the maximum Δx achievable is less than 5 g/kg. Performance is better at T_{reg} 80 °C where the maximum Δx is higher than 7 g/kg. The rate of increase in latent cooling does not benefit from significant increase in heat source temperature level. Optimal revolution speed is slightly affected by regeneration temperature with fixed AR. However, ω^{opt} varies a lot with area ratio. In Table 4 the value of AR and the corresponding ω^{opt} is reported for different regeneration temperature and process air

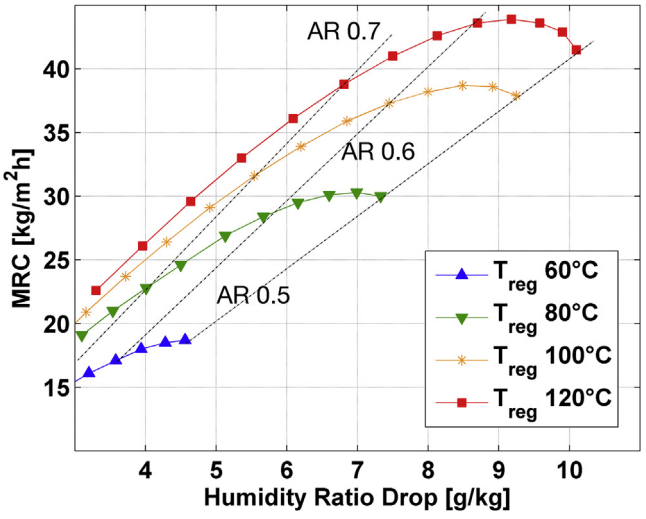

Fig. 5. Moisture Removal Capacity as a function of Humidity Ratio Drop. Dashed lines connecting points at the same value of area ratio value. T_{pro} 30 °C, x_{in} 15 g/kg, v 2 m/s.

Table 4
Optimal revolution speed as a function of T_{reg} and Δx.

T_{reg} [°C]	Δx 3 g/kg		Δx 5 g/kg		Δx 7 g/kg	
	AR	ω^{opt}	AR	ω^{opt}	AR	ω^{opt}
60	0.62	50	–		–	–
80	0.75	20	0.65	45	0.53	50
100	0.80	15	0.71	30	0.62	40
120	0.84	10	0.76	25	0.68	30

humidity ratio drop. Optimal revolution speed ranges between 15 and 50 RPH.

The global behaviour of MRC in relation to Δx and AR is almost independent of the process air flow inlet conditions. For instance, Fig. 6 provides desiccant wheel latent cooling for high humidity scenario (T_{pro} 35 °C x_{pro} 25 g/kg) with same face velocity. MRC is comparable with mild humidity scenario since for the same values of AR and T_{reg} and slightly greater values are found only in the high temperature range. A larger amount of dehumidification is observed and a flatter plateau zone is achieved in the high temperature range for 0.5 < AR < 0.6. Optimal revolution speed does not vary considerably compared with mild humidity scenario.

5.2. Effect of process air temperature and humidity

In this subsection an equal area split is considered to investigate the effect of outdoor conditions. In order to discuss the effect of inlet temperature and humidity ratio the following indexes are defined as below in Eqs.(29) and (32)

$$MRE = \frac{x_{pro}^{in} - x_{pro}^{out}}{x_{pro}^{in}} \tag{29}$$

$$MRE^{*} = \frac{MRE}{MRE_{ref}} \tag{30}$$

$$\Delta T_{pro} = T_{pro}^{out} - T_{pro}^{in} \tag{31}$$

$$\Delta T^{*} = \frac{\Delta T_{pro}}{\Delta T_{ref}} \tag{32}$$

where the reference Moisture Removal Efficiency (MRE_{ref}) and reference temperature difference (ΔT_{ref}) are calculated at process inlet reference temperature T_{ref} of 30 °C. This has been proposed as a practically useful index to distinguish the effect of process inlet temperature from humidity ratio.

In Figs. 7 and 8 it is provided the effect of inlet humidity ratio on MRE and ΔT_{pro} respectively for different level of T_{reg}. MRE decreases almost linearly with $x_{in,}$ since MRC for fixed AR and T_{reg} is relatively constant regardless of air flow inlet conditions (as shown in Figs. 5 and 6). The temperature rise of process air increases with increasing inlet humidity. This increase is more pronounced at the higher regeneration temperatures. Relatively small increase in process air temperature is noted for T_{reg} below 80 °C, and this is consistent with the fact that MRC tend to be constant regardless of the process inlet flow conditions. Only for T_{reg} >80 °C dehumidification increases substantially with inlet humidity ratio.

When process air inlet temperature is varied ±5 °C from the reference temperature, it is found that MRE and ΔT_{pro} can experience variation up to 10% and 15% respectively in comparison with the reference case as shown in Figs. 9 and 10. The effect is most significant for T_{reg} 60 °C and dry inlet air flow, leading to the greatest variation in MRE in comparison with the reference temperature scenario. For higher regeneration temperatures, the discrepancy between the actual and reference case is smaller and tends to be constant with inlet humidity. This is consistent with the fact that higher values of x_{in} can be detrimental for dehumidification performance if a low grade heat source is adopted.

5.3. Effect of face velocity on optimal revolution speed

The influence of face velocity on desiccant wheel performance needs to be taken into account, since variable air volume systems either can be designed with different air flow velocity or operate at part load reducing volume flow rate.

In the following analysis, area ratio is set equal to 0.5 with balanced flow face velocities, therefore maximizing MRC implies finding maximum Δx. Here the effect of revolution speed on the

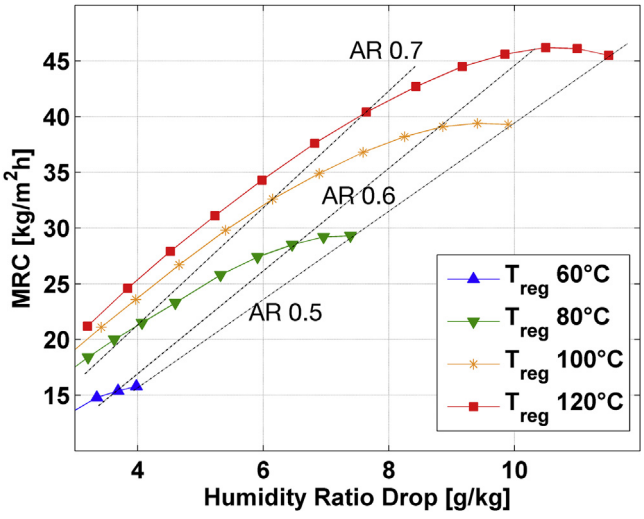

Fig. 6. Moisture Removal Capacity as a function of humidity ratio drop. Dashed lines connect points at the same value of area ratio. T_{pro} 35 °C, x_{pro} 15 g/kg scenario, v 2 m/s.

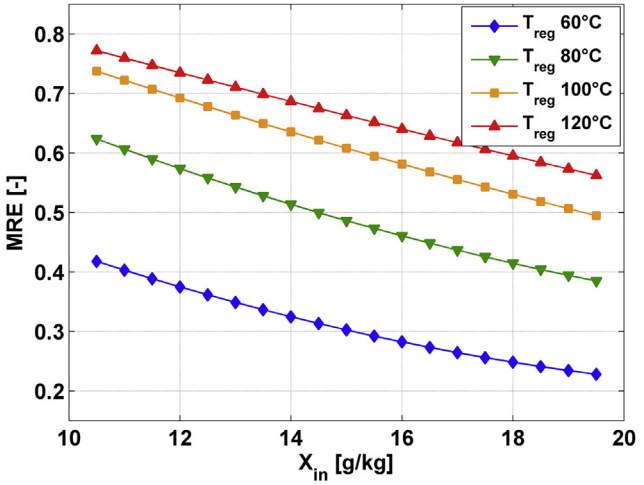

Fig. 7. MRE for different level of T_{reg} as a function of inlet humidity ratio x_{in} (set equal for both process and regeneration flow). AR 0.5, v 2 m/s, process inlet reference temperature 30 °C.

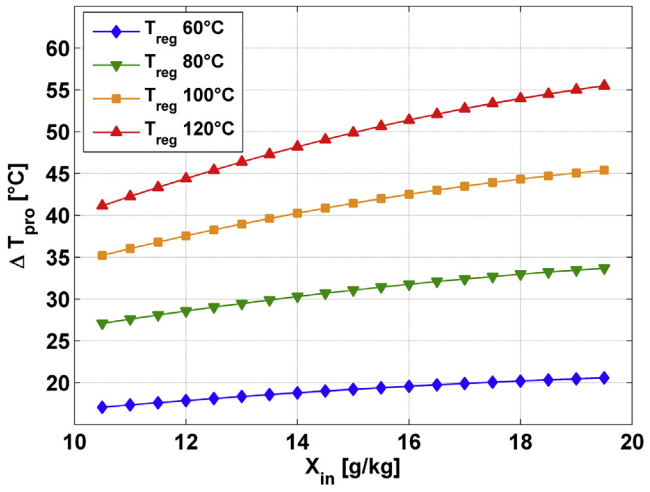

Fig. 8. Process air rise in temperature as a function of inlet humidity ratio x_{in} (set equal for both process and regeneration flow). AR 0.5, v 2 m/s, process inlet reference temperature 30 °C.

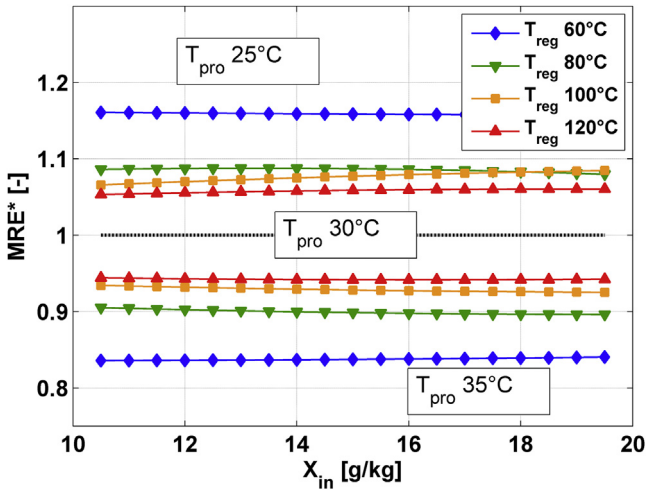

Fig. 10. Actual to reference process increase in temperature ratio as a function of inlet humidity ratio x_{in} (set equal for both process and regeneration flow). AR 0.5, v 2 m/s, process inlet reference temperature 30 °C.

amount of moisture removed is numerically investigated for different inlet velocities.

Optimal revolution speed ω^{opt} increases with inlet velocity (and therefore volume flow rate) as shown in Figs. 11 and 12. This is because a larger volume flow leads to a faster saturation of the desiccant bed; therefore a higher revolution speed is required to remove moisture from the wet desiccant layer. Increasing face velocity brings about a weaker dependency on revolution speed: referring to face velocity ranging from 2 to 3 m/s (Figs. 11 and 12) dehumidification is almost constant over a wide range of revolution speeds and falls down substantially only for ω below 20RPH. On the other hand with low face velocity (v 1 m/s) moisture removal is much more sensitive to revolution speed and a significant drop in performance occurs whether ω is either higher or lower than ω^{opt}, which is about 10–15 RPH (Figs. 11–12). Optimal revolution speed turns out to increase slightly with regeneration temperature.

Several works have focused on optimal revolution speed [1,3,4,10,22,30] and few authors proposed non dimensional parameters to link optimal revolution speed to main flow quantities [31,32]. In this work *Dwell time* and *non-dimensional moisture removal* are adopted and defined in Eqs. (33) and (34)

$$\tau_D = \omega' L / v \tag{33}$$

$$\Delta x^* = \Delta x / \Delta x^{max} \tag{34}$$

where Δx^{max} is the maximum achievable humidity ratio drop [g/kg] given regeneration temperature and flow inlet velocity. The relationship between these new parameters was investigated at three air velocities (Figs. 13 and 14). Dwell time appears to be a reasonably good parameter to predict optimal revolution speed as a function of face velocity as long as T_{reg} is moderately high. Optimal operating conditions are located in quite a narrow zone for (τ_D*3600) between 2 and 3.5 and between 2.5 and 4 for 80 °C and 100 °C regeneration temperatures, respectively. The overall trend of Δx^* is almost independent of regeneration temperature, as displayed in Fig. 14. Little discrepancy is observed for moisture removed at different inlet velocity for (τ_D*3600) > 5, however this

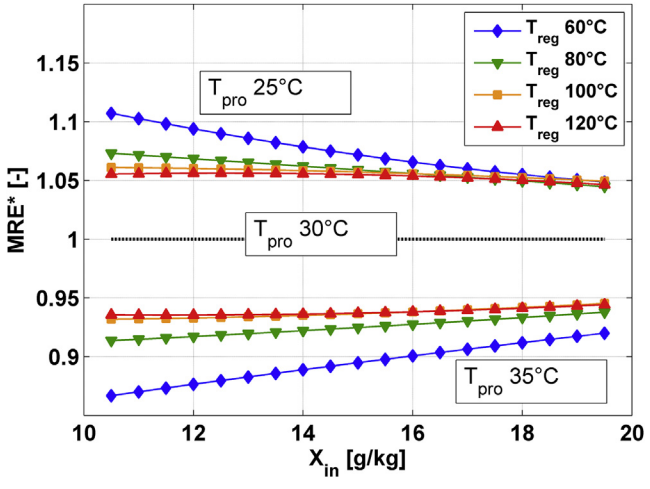

Fig. 9. Actual to reference moisture removal efficiency ratio as a function of inlet humidity ratio x_{in} (set equal for both process and regeneration flow). AR 0.5, v 2 m/s, process inlet reference temperature 30 °C.

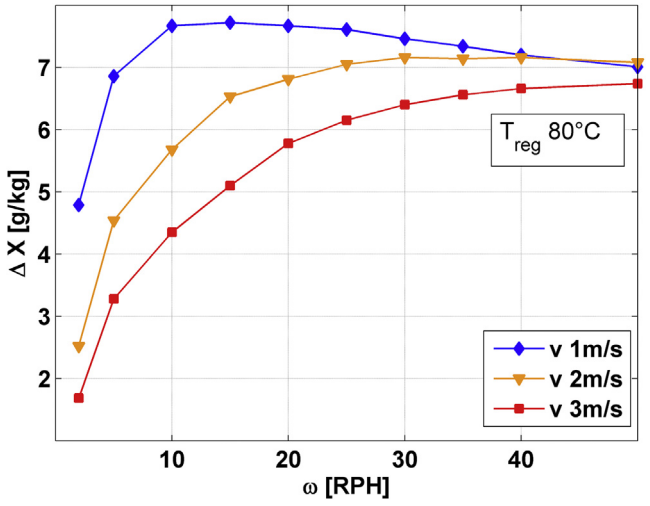

Fig. 11. Humidity ratio drop as a function of revolution speed (T_{pro} 30 °C, x_{in} 15 g/kg, T_{reg} 80 °C, AR 0.5).

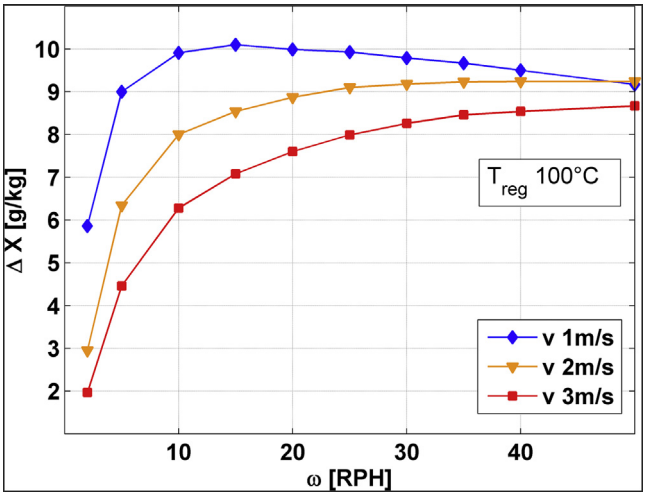

Fig. 12. Humidity ratio drop as a function of revolution speed (T_{pro} 30 °C, x_{in} 15 g/kg, T_{reg} 100 °C, AR 0.5).

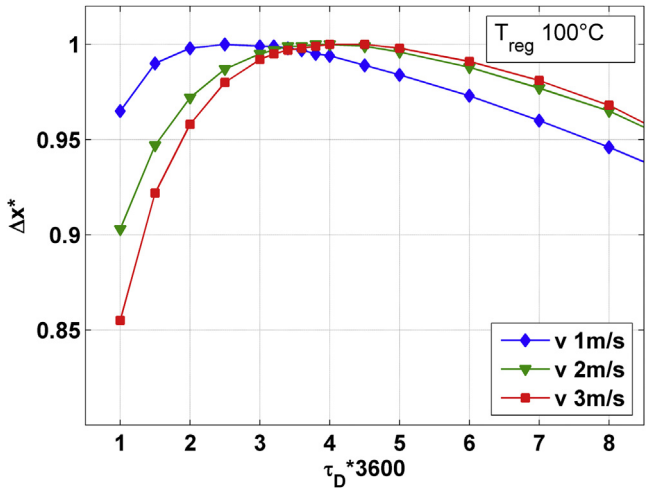

Fig. 14. Non-dimensional moisture removal as a function of dwell time: effect of inlet surface velocity (T_{pro} 30 °C, x_{pro} 15 g/kg, AR 0.5).

occurs far from the optimal range zone. This suggests a very useful method to predict simple control strategies when the face velocity is varied significantly from the design value.

6. Conclusions

In the present work the dehumidification performance of a novel generation of zeolite-based desiccant wheel has been investigated. The desiccant wheel has been experimentally characterized in a wide range of inlet humidity and regeneration temperature conditions. A gas–solid side resistance model has been developed and calibrated to predict desiccant wheel outlet performance in cyclic conditions. The effect of area ratio, face velocity, process air temperature and humidity are investigated and non-dimensional parameters to predict optimal revolution speed are proposed.

It is found that for fixed inlet velocities and constant regeneration temperature, moisture removal capacity increases with humidity ratio drop. Maximum moisture removal capacity is achieved when the highest humidity ratio drop is obtained and this occurs with AR 0.5 in the low-medium range of temperature. Only for high grade regeneration heat (T_{reg} >100 °C) maximum removal capacity can be attained with 0.5 < AR < 0.6. This suggests that this material is most suitable for medium and high temperature applications with regeneration temperature ranging between 80 °C and 100 °C.

Outdoor humidity conditions can significantly affect dehumidification efficiency, which tends to decrease for very damp air streams. Variation in process inlet temperature at constant inlet humidity ratio turns out to affect barely moisture removal efficiency and this effect can be considered negligible for very wet flows.

Optimal revolution speed is strongly affected by area ratio, the higher AR, the higher ω^{opt}. When the area ratio ranges from 0.5 to 0.8 and regeneration temperatures is between 60 °C and 120 °C, ω^{opt} is between 10RPH and 50 RPH depending on the targeted humidity ratio drop. If AR is equal to 0.5, ω^{opt} is mainly a function of face velocity with a weak influence on regeneration temperature. Non dimensional analysis shows that optimal revolution speed can be found in a relatively narrow range when the dwell-time τ_D*3600 is close to 3–4. Dwell-time turns out to be a simple parameter to predict ω^{opt} which maximizes moisture removal capacity with acceptable accuracy. This may suggest strategy for desiccant wheel control at part load condition.

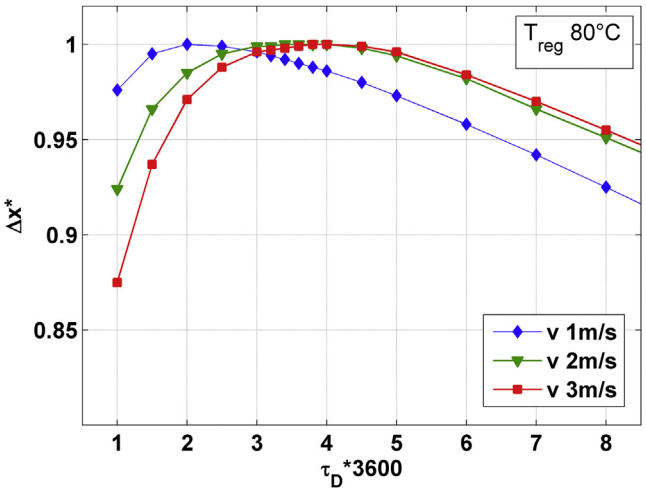

Fig. 13. Variation of non-dimensional moisture removal as a function of dwell time: effect of inlet surface velocity (T_{pro} 30 °C, x_{pro} 15 g/kg, AR 0.5).

Acknowledgements

This work was funded by CSIRO and the Australian Renewable Energy Agency. The authors would like to acknowledge Roger Reece and Mark Peristy for providing assistance on the experimental facility.

Nomenclature

a	channel height [mm]
A_C	channel inner surface area [m^2]
A_{DW}	desiccant wheel cross section area [m^2]
AR	process to total cross section area ratio [–]
b	channel width [mm]
c	wall half thickness [mm]
c_p	specific heat [J kg^{-1} K^{-1}]
D	diffusivity [m^2 s^{-1}]

D_H	hydraulic diameter [m]
f_D	mass fraction of desiccant in the solid domain [kg kg^{-1}]
Gz	Graetz number [−]
h_M	convective mass transfer coefficient[kg m^{-2} s^{-1}]
h_T	convective heat transfer coefficient [kg m^{-2} s^{-1}]
k	thermal conductivity [W m^{-1} K^{-1}]
k_0	Toth constant [kPa^{-1}]
L	channel length [m]
m	dry air mass flow rate [kg s^{-1}]
MRC	moisture removal capacity [kg s^{-1} m^{-2}]
MRE	moisture removal efficiency [−]
MRE*	actual to reference temperature moisture removal efficiency
Nu	Nusselt number [−]
n	Toth correlation exponents [−]
p_{atm}	atmospheric pressure [Pa]
p_v	water vapour partial pressure [Pa]
P	channel inner perimeter [m]
Pr	Prandtl number [−]
Q	cooling capacity [W]
Q_{st}	isosteric heat of adsoption [W]
r_p	average pore radius [m]
R	water gas constant [J kg^{-1} K^{-1}]
Re	Reynolds number [−]
RH	relative humidity [%]
Sh	Sherwood number [−]
t	time [s]
$\tilde{T}$	absolute temperature [K]
T	temperature [°C]
u	air channel velocity [m s^{-1}]
v	face velocity [m s^{-1}]
x	humidity ratio [kg$_v$ kg$_{da}^{-1}$]
W	adsorbed water per unit mass of desiccant [kg kg$_{ads}^{-1}$]
z	axial coordinate [m]

Greek symbols

δT	temperature sensor accuracy [°C]
Δx	process air humidity ratio drop [g/kg]
Δx^*	non dimensional moisture removal [−]
ε	void fraction [−]
ΔH_{ev}	water latent heat of vaporization [J kg^{-1}]
ρ	density [kg m^{-3}]
Ψ	generic physical quantity
τ_D	dwell time [−]
ω	desiccant wheel revolution speed [RPH]
$\dot{\omega}$	desiccant wheel angular frequency [s^{-1}]

Subscripts and superscripts

a	dry air
ave	average
b	bulk
cyc	cycle (process and regeneration stage)
d	desiccant
fd	fully developed
in	inlet
lat	latent
max	maximum
o	ordinary
kn	Knudsen
opt	optimal
out	outlet
pro	process
reg	regeneration
s	solid domain, surface (for diffusion)
w	water

References

[1] S. De Antonellis, L. Molinaroli, C. Joppolo, Simulation, performance analysis and optimization of desiccant wheels, Energy Build. 42 (2010) 1386–1393.

[2] S. De Antonellis, C. Joppolo, L. Molinaroli, A. Pasini, Simulation and energy efficiency analysis of desiccant wheels for drying process, Energy 37 (2012) 336–345.

[3] A. Kodama, M. Goto, T. Hirose, Experimental study of optimal operation for a honeycomb adsorber operated with thermal swing, J. Chem. Eng. Jpn. 27 (1994) 644–649.

[4] A. Kodama, T. Hirayama, M. Goto, T. Hirose, R. Critoph, The use of psychometric charts for the optmization of a thermal swing desiccant wheel, Appl. Therm. Eng. 21 (2001) 1657–1674.

[5] H.T. Chua, K.C. Ng, A. Chakraborty, N.M. Oo, M.A. Othman, Adsorption characteristics of silica gel + water systems, J. Chem. Eng. Data 47 (2002) 1177–1181.

[6] B. Dawoud, Y.I. Aristov, Experimental study on the kinetics of water vapour sorption on selective water sorbents, silica gel and alumina under typical operating conditions of sorption heat pumps, Int. J. Heat Mass Transf. 46 (2003) 273–281.

[7] Y.I. Aristov, G. Restuccia, G. Cacciola, V. Parmon, A family of new working materials for solid sorption air conditioning systems, Appl. Therm. Eng. 22 (2002) 191–204.

[8] Y. Aristov, New family of solid sorbents for adsorptive cooling: material science approach, J. Eng. Thermophys. 16 (2007) 63–72.

[9] X. Zhang, K. Sumathy, Parametric study on the silica gel − calcium chloride composite desiccant rotary wheel employing fractal BET adsorption isotherm, Int. J. Energy Res. 29 (2005) 37–51.

[10] T. Ge, F. Ziegler, A mathematical model for predicting the performance of a compound desiccant wheel, Appl. Therm. Eng. 30 (2010) 1005–1015.

[11] A. Dieng, R. Wang, Literature review on solar adsoprtion technologies for ice-making and air-conditioning purposes and recent developments in solar technology, Renew. Sustain. Energy Rev. 5 (2001) 313–342.

[12] M. Clausse, F. Meunier, J. Coulié, E. Herail, Comparison of adsorption systems using natural gas fired fuel cell as heat source for residential air conditioning, Int. J. Refrig. 32 (2009) 712–719.

[13] B. Sun, A. Chakraborty, Thermodynamic formalism of water uptakes on solid adsorbents for adsorption cooling applications, Appl. Phys. Lett. 104 (2014) 201901.

[14] H. Kakiuki, K. Ooshima, Novel zeolite adsorbents ad their application for AHP and desiccant system, in: Proceedings of the IEA Expert Meeting, 2004. Kizkalesi, Turkey.

[15] M. Llano-Restrepo, M. Mosquera, Accurate correlation, thermochemistry and structural interpretation of equilibrium adsorption isotherms of water vapour in zeolite 3A by means of a generalized statistical thermodynamic adsorption model, Fluid Phase Equilibr. 283 (2009) 73–88.

[16] A. Pesaran, A. Mills, Moisture transport in silica gel packed bed. I theoretical study, Int. J. Heat Mass Transf. 30 (1987) 1037–1049.

[17] M.J. Goldsworthy, Measurements of water vapour sorption isotherms for RD silica gel, AQSOA-Z01, AQSOA-Z02, AQSOA-Z05 and CECA zeolite 3A, Micropor. Mesopor. Mater. 196 (2014) 59–67.

[18] A. Frazzica, A. Sapienza, A. Freni, Novel experimental methodology for the characterization of thermodynamic performance of advanced working pairs for adsorptive heat transformers, Appl. Therm. Eng. 72 (2014) 229–236.

[19] B. Dawoud, Water vapor adsorption kinetics on small and full scale zeolite coated adsorbers; a comparison, Appl. Therm. Eng. 50 (2013) 1645–1651.

[20] U. Eicker, U. Schurger, M. Koler, T. Ge, Y. Dai, H. Li, R. Wang, Experimental investigations on desiccant wheels, Appl. Therm. Eng. 42 (2012) 71–80.

[21] S. White, M. Goldsworthy, Characterization of desiccant wheel with alternative materials at low regeneration temperature, Int. J. Refrig. 34 (2011) 1786–1791.

[22] W. Cho, K. Shinsuke, O. Ryozo, Study on dehumidification performance of FAM-Z rotor, in: Proceedings 6th International Conference on Indoor Air Quality, Ventilation and Energy Conservation in Buildings, 2007. Sendai, Japan.

[23] T. Ge, Y. Li, R. Wang, Y. Dai, A review of the mathematical models for predicting rotary desiccant wheel, Renew. Sustain. Energy Rev. 12 (2008) 1485–1528.

[24] C. Ruivo, J. Costa, A. Figureido, On the behaviour of hygroscopic wheels: part I − channel modeling, Int. J. Heat Mass Transf. 50 (2007) 4812–4822.

[25] T. Yamamoto, Y. Kim, B. Kim, A. Endo, N. Thongprachan, T. Ohmori, Adsorption characteristics of zeolites for dehydration of ethanol: evaluation of diffusivity of water in porous structure, Chem. Eng. J. 1 (2012) 443–448.

[26] M. Goldsworthy, S. White, Optimization of a desiccant cooling system design with indirect evaporative cooler, Int. J. Refrig. 34 (2011) 148–158.

[27] S. Kakaç, R. Shah, W. Aung, Handbook of Single Phase Convective Heat Transfer, John Wiley & Sons, New York, 1987.

[28] J. Niu, L. Zhang, Heat transfer and friction coefficient in corrugated ducts confined by sinusoidal and arc curves, Int. J. Heat Mass Transf. 45 (2002) 571–578.
[29] ASHRAE Standard 139, Method of Testing for Rating Desiccant De-humidifiers Utilizing Heat for the Regeneration Process, American Society of Heating, Refrigerating, and Air-Conditioning Engineers, Atlanta, Georgia, 1998.
[30] L. Zhang, J. Niu, Performance comparisons of desiccant wheels for air dehumidification and enthalpy recovery, Appl. Therm. Eng. 22 (2002) 1347–1367.
[31] M. Golubovic, H. Madhawa Hettiarachchi, W. Worek, Evaluation of rotary dehumidifier performance with and without heated purge, Int. Commun. Heat Mass Transf. 34 (2007) 785–795.
[32] L. Sphaier, W. Worek, Analysis of heat and mass transfer in porous sorbents used in rotary regenerators, Int. J. Heat Mass Transf. 47 (2004) 3415–3430.